Force-matching-based parameterization of the Stillinger-Weber potential for thermal conduction in silicon

Yongjin Lee and Gyeong S. Hwang*
Department of Chemical Engineering, University of Texas, Austin, Texas 78712, USA
(Received 20 July 2011; revised manuscript received 21 November 2011; published 22 March 2012)

A force-matching method is employed to optimize the parameters of the Stillinger–Weber (SW) interatomic potential for calculation of the lattice thermal conductivity of silicon. The parameter fitting is based on first-principles density functional calculations of the restoring forces for atomic displacements. The thermal conductivities of bulk crystalline Si at 300–500 K estimated using nonequilibrium molecular dynamics with the modified parameter set show excellent agreement with existing experimental data. We also briefly discuss how the force-matching-based parameterization can provide the improved estimation of thermal conductivity, as compared to the original SW parameter set, through analysis of phonon density of states and phonon dispersion relations.

DOI: 10.1103/PhysRevB.85.125204 PACS number(s): 65.40.−b

I. INTRODUCTION

Thermal conductivity is an important property in many applications including microelectronics and thermoelectrics. In particular, the efficiency of thermoelectric devices that convert heat energy to electricity is a direct function of thermal conductivity;[1–4] that is, a figure of merit (ZT) value, or efficiency measure, is given in terms of thermal (κ) and electrical (σ) conductivities, $ZT = S^2\sigma T/\kappa$, where T is the absolute temperature and S the Seebeck coefficient.[5] Over the last few years, significant efforts have been undertaken to improve the thermoelectric efficiency of silicon (Si)-based materials by reducing the thermal conductivity through alloying, doping, and nanostructuring; but further efficiency enhancement is still necessary to compete with conventional thermodynamic devices. In addition, with the continuous reduction of feature size, thermal management has become an important issue in the current and future fabrication of microelectronic devices.[6]

Thermal conductivity measurement of nanostructured materials and devices is still challenging because of technical difficulties in synthesis of high-quality well-ordered nanostructures as well as characterization of individual nanostructural elements affecting thermal conduction and complex geometries of real devices.[7] Hence, there has been much interest in use of theoretical and computational methods to investigate the thermal properties of nanoscale materials and devices. Classical molecular dynamics (MD) simulations with empirical force fields have been widely applied to estimate thermal conductivity of various materials and structures, such as bulk,[8,9] nanoparticles,[10] and nanotubes,[11] and also to investigate how structural imperfections, such as defects,[12,13] impurities,[14] surfaces,[15–17] and disordered alloys[18] affect lattice thermal conductivity.

Empirical force fields, such as three-body Stillinger–Weber (SW)[19] and Tersoff[20] interatomic potentials, have been successfully employed to study the structural, energetic, and mechanical properties of Si-based materials.[21,22] However, their description of lattice dynamics is often unsatisfactory despite its importance in assessing thermal transport properties;[23] for instance, previous MD simulations based on original SW and Tersoff parameters yielded significant overestimates of Si thermal conductivity, i.e. 235.7 ± 7.5 $\mathrm{Wm^{-1}K^{-1}}$ at 300 K (Tersoff[13]) and 119 ± 40 $\mathrm{Wm^{-1}K^{-1}}$ at 500 K (SW[8]), as compared to experimental values of 130 W/mK at 300 K and 76.2 $\mathrm{Wm^{-1}K^{-1}}$ at 500 K.[24] It is likely an insurmountable task to generate a single force field that can provide an adequate description of all physical and chemical properties, even for a prototypical semiconductor like Si. Therefore, it would be necessary to at least modify existing force fields for specific applications, such as lattice thermal conductivity calculations.

While lattice dynamics directly depend on force constants between atoms,[25] earlier studies demonstrated substantial improvement in description of lattice dynamical properties through modification of relevant force constants. Jian *et al.*[26] showed that the SW potentials modified to fit the available experimental values of bulk modulus and phonon frequencies (particularly optical mode at the Γ point and transverse acoustic mode at the X point) yielded considerably improved phonon-dispersion relations for Si and Ge. Very recently, Lindsay and Broido[27] presented improved Tersoff and Brenner potential parameters for phonon thermal transport in carbon nanotubes and graphene that were optimized to better fit measured phonon frequencies and zone-center acoustic velocities.

In this paper, we use a force-matching method to optimize the parameters of the SW empirical interatomic potential for lattice thermal transport in Si. The SW parameters are adjusted to obtain a better fit of density functional theory (DFT) calculations of the lattice, restoring forces arising from local lattice distortions. Using nonequilibrium molecular dynamics (NEMD) with the modified SW parameters, we calculate the thermal conductivities of bulk crystalline Si (c-Si) for different temperatures and compare the results with those obtained with the original parameters as well as existing experimental data. Through comparison of calculated phonon density of states and phonon dispersion relations to experimental observations, we also attempt to discuss how the optimized parameter set provides improved agreement with measured values of thermal conductivity.

II. THEORY

A. Stillinger–Weber interatomic potential

Within the Stillinger–Weber potential (Ref. 18), the total energy (Φ) is given by the sum of two- (Φ_2) and three-body

(Φ_3) interactions:

$$\Phi(r) = \sum_{i,j(i<j)} \Phi_2(r_i,r_j) + \sum_{i,j,k(i<j<k)} \Phi_3(r_i,r_j,r_k) \quad (1)$$

The two-body potential (Φ_2) is a function only of radial distance (r), described in terms of a combination of inverse powers and an exponential function [Eq. (2)], and the three-body potential possess full translational and rotational symmetry to give a diamond structure of solid silicon, given as the product exponential and cosine functions [Eq. (3)].

$$\Phi_2(r_{ij}) = \begin{cases} \varepsilon A\left(Br_{ij}^{-p} - r_{ij}^{-q}\right)\exp[1/(r_{ij}-a)], & r_{ij} < a \\ 0 \quad r_{ij} \geqslant a \end{cases} \quad (2)$$

$$\begin{aligned} \Phi_3(r_i,r_j,r_k) &= h(r_{ij},r_{ik},\theta_{ijk}) + h(r_{ij},r_{jk},\theta_{ijk}) \\ &\quad + h(r_{ki},r_{kj},\theta_{ikj}); \\ h(r_{ij},r_{ik},\theta_{jik}) &= \varepsilon\lambda\exp[\gamma/(r_{ij}-a) \\ &\quad + \gamma/(r_{ik}-a)](\cos\theta_{jik} + 1/3)^2 \end{aligned} \quad (3)$$

where the subscripts ij, ik, and jik represent pairs and triplets involving atoms i, j, and k; r_{ij} is the interatomic distance between atoms i and j (normalized by a characteristic length σ); and θ_{ijk} is the angle between bonds ij and ik.

In the original study, the seven parameters (A, B, p, q, a, λ, and γ) were adjusted to give a diamond lattice structure in the solid state and fit molecular dynamics simulation results to experimental observations for melting temperature and liquid structure. In addition, the values of σ and ε were chosen to match the observed lattice constant and atomization energy of crystalline Si at 0 K, respectively. Although the SW potential overall gives a fairly realistic description of crystalline Si, as stated earlier, the thermal conductivities calculated based on the original SW parameters[18] tend to be overestimated. Since lattice dynamics directly depend on force constants between atoms,[25] this implies that the original set of parameters may describe the Si lattice as somewhat rigid, which is probably related to the fact that the energy-scaling parameter (ε) was fitted to the atomization energy at 0 K. Note that thermal conduction at a finite temperature inherently involves lattice fluctuations, e.g. the mean atomic displacement in c-Si is about 0.077 Å at room temperature;[28] such thermal-induced lattice distortions would lead to a softening of the lattice and consequently require smaller force constants in describing the thermal transport properties near or above room temperature.

B. Parameter optimization using a force-matching method

To improve the description of lattice dynamics, using a force-matching method,[29] we adjusted three SW parameters (σ, ε, and λ) to fit DFT results for both the lattice spacing and the lattice restoring forces arising from local lattice distortions. The values of σ were chosen to match the LDA/GGA lattice constants for the Si diamond structure. In the SW potential, εA and $\varepsilon\lambda$ determine the relative strength between the two- and three-body interactions. Since A is preset, ε and λ were tuned to fit the DFT restoring forces.

Our DFT calculations were performed within the local density approximation (LDA) and the Perdew–Wang 91 generalized gradient approximation (GGA-PW91),[30] using the Vienna *ab initio* Simulation Package (VASP).[31] We used Vanderbilt-type ultrasoft pseudopotentials[32] to represent the interaction between ion cores and valence electrons, and a plane-wave basis set with a kinetic energy cutoff of 160 eV. We used a 64-atom cubic supercell and a $(2 \times 2 \times 2)$ k-point grid in the scheme of Monkhorst–Pack for the Brillouin zone sampling. The predicted GGA (LDA) Si lattice constants are 5.4571 (5.3865) Å, which were used for MD simulations.

TABLE I. Parameters of the Stillinger–Weber interatomic potential in Eqs. (2) and (3); original[19] [SW(ORI)] and modified values based on fit to GGA [SW(GGA)] and LDA [SW(LDA)] calculations (this paper).

	σ	ε (eV)	λ	
SW(ORI)	2.0951	2.1683	21	$A = 7.049556277$
SW(GGA)	2.1051937	1.41992	29.5304	$B = 0.6022245584$
SW(LDA)	2.0780213	1.49662	26.4091	$\gamma = 1.2, a = 1.8$
				$p = 4.0, q = 0.0$

The DFT force data for parameter optimization were obtained by displacing one atom in the x, y, and z directions by 0.2 Å; the magnitude of the displacements was carefully determined from test calculations with different values which were greater than the mean atomic displacement of about 0.077 Å in c-Si at 300 K.[28] The restoring forces acting on the displaced atom and its four first- and 12 second-nearest neighbors were considered to be matched in the SW parameter adjustments. On the third-nearest neighbors and beyond, the forces due to the center-atom displacement are negligible (<0.01 eV/Å in the absolute value). The optimal values for ε and λ were obtained through minimization of the cross-validation error (ξ); $\xi^2 = \frac{1}{N}\sum_{n=1}^{N}(F_{\rm DFT}^{(n)} - F_{\rm SW}^{(n)})^2$, where $F_{\rm DFT}^{(n)}$ and $F_{\rm SW}^{(n)}$ refer to the DFT and SW forces, respectively, of the nth of N total training data for force matching.

Table I summarizes the modified parameters based on GGA [SW(GGA)] and LDA [SW(LDA)] calculations, together with the original parameters [SW(ORG)] for comparison. In Fig. 1, we compare the restoring forces from the SW and DFT calculations; both SW(GGA) and SW(LDA) reproduce the

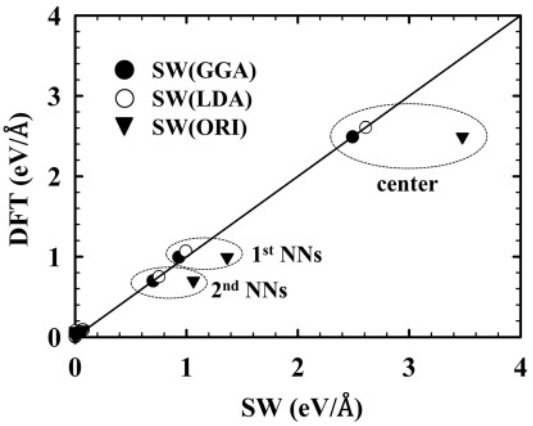

FIG. 1. Discrepancies between DFT and SW predictions for the restoring forces acting on the displaced atom (center) and its four first- (1st NNs) and 12 second-nearest neighbors (2nd NNs).

DFT forces acting on the center atom and its neighbors well, while SW(ORG) yields consistently overestimated values. In the three-body SW potential, the forces can be decoupled into two- (F) and three-body (G) contributions; that is, $F = \frac{1}{3\sigma^2}\frac{d^2\Phi_2}{dr^2}|_{r=2^{1/6}}$ and $G = \frac{8\varepsilon\lambda}{27\sigma^2 r^2}\exp(\frac{2r}{r-a})|_{r=2^{1/6}}$, where σ, ε, λ, and a are the SW parameters [see Eqs. (1)–(3)]. Looking at the relative two- and three-body forces of SW(GGA) and SW(LDA) with respect to SW(ORI), there is a significant reduction in the two-body forces ($\gamma_F = 0.65/0.70$ for GGA/LDA), while the three-body force reduction is relatively smaller ($\gamma_G = 0.91/0.88$ for GGA/LDA). The decrease of forces indicates that SW(GGA) and SW(LDA) will describe the Si lattice as softer than SW(ORI).

C. Nonequilibrium molecular dynamics

With the modified parameters, we performed nonequilibrium molecular dynamics (NEMD) simulations using LAMMPS[33] to estimate the thermal conductivity of c-Si and compared the results with those obtained with the original parameters. Thermal conductivity (κ) is given, according to Fourier's law, by $\kappa = -J/\Delta T$; in the NEMD approach, the temperature gradient (ΔT) is obtained by imposing the heat flux (J) or vice versa. The temperature in an MD simulation ($T_{\rm MD}$) is commonly calculated from the velocities of constituent atoms based on the equipartition theorem of classical statistical mechanics: $\frac{3}{2}Nk_BT_{\rm MD} = \frac{1}{2}\sum_{i=1}^{N} mv_i^2$, where N is the number of atoms in the system, k_B is the Boltzmann constant, v_i is the velocity of atom i, and m is the atomic mass. If $T_{\rm MD}$ is far below the Debye temperature, quantum corrections to the MD temperature and thermal conductivity ($\kappa_{\rm MD}$) are necessary; the corrected thermal conductivity is given by $\kappa = \kappa_{\rm MD}\frac{dT_{\rm MD}}{dT}$.[34]

As depicted in Fig. 2, we employed a rectangular-shaped simulation domain with periodic boundary conditions imposed in the x, y, and z directions, where heat conduction occurs in the z (or ⟨100⟩) direction. Fixed lattice constants of 5.4571 Å (GGA) and 5.3865 Å (LDA) along ⟨100⟩ were used; hereafter, only GGA values will be reported, and corresponding LDA values are scaled accordingly. The cross-sectional area of each simulation domain is 3.8405×3.8405 nm^2, while the domain is axially divided into a number of thin shells (each of which contains 400 atoms). The thickness of the heat source and heat sink layers is set to $L_S = 5.4571$ Å (corresponding to one shell in the axial direction or 400 atoms), and the total axial length of the rectangular domain varies from $L_{\rm tot} = 65.485$, 87.313, 109.142, and 130.97, to 174.627 nm (corresponding to 120, 160, 200, 240, and 320 shells, respectively).

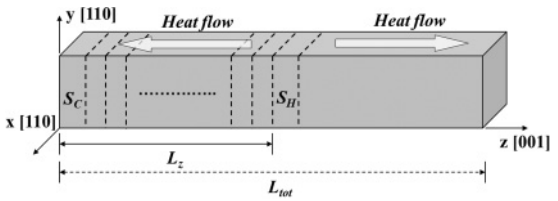

FIG. 2. Schematic illustration of a rectangular-shaped simulation domain with periodic boundary conditions imposed in the x, y, and z directions, where heat conduction occurs in the z (or [100]) direction. The simulation domain is axially divided into a number of thin shells (each of which contains 400 atoms) while having heat source (S_H) and heat sink (S_C) layers, as indicated.

In the direct method, if the axial length of the simulation domain is not sufficiently larger than the mean free path of phonons, the phonon scattering in the heat sink and heat source layers could inhibit thermal conduction, thereby underestimating thermal conductivity. The finite-size effect can be removed by extrapolating to the infinite size limit. Note that, according to Schelling *et al.*,[8] the relationship between size-dependent thermal conductivity and simulation domain length ($L_{\rm tot} = 2L_z$, where L_z is the distance between the heat source and heat sink centers, which is half of the total simulation domain length) is given by: $\frac{1}{\kappa} \propto (\frac{1}{l_\infty} + \frac{2}{L_z})$, where l_∞ is the phonon mean free path for the infinite system. We expect that the linear extrapolation approach would work reasonably well if the simulation domain size is sufficiently large and the system is fully equilibrated, but cannot exclude the possibility that it may cause some errors in estimation of bulk thermal conductivity; nonetheless, this insignificantly affects the evaluation of the effectiveness of potential parameter sets.

III. RESULTS AND DISCUSSION

As shown in Fig. 3, we calculated the bulk thermal conductivities of c-Si by extrapolating calculated $(1/L_z, 1/\kappa)$ values to $1/L_z = 0$. For each system, we performed 10 independent NEMD simulations with different initial velocity distributions to obtain good statistics; the system was initially equilibrated at a target temperature within the canonical (NVT) ensemble with a Nosé–Hoover thermostat for 100 ps, followed by 2000 ps of microcanonical (NVE) MD while imposing a heat flux (with a velocity swap interval of 100 MD steps) and measuring the ensuing temperature gradient. A time step of 1 fs was adopted for all MD simulations reported herein. Each calculated temperature profile was obtained by averaging over 10^5 MD steps (100 ps) after equilibrium was reached. Those

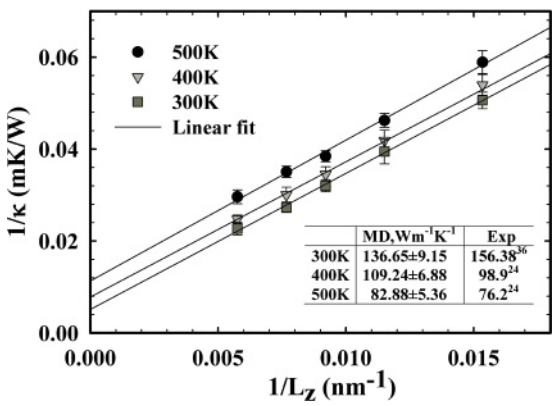

FIG. 3. Thermal resistivity ($1/\kappa$, after quantum corrections) for c-Si as a function of simulation cell length at three different temperatures as indicated; for each set, the linear line indicates the best-fit linear regression. Here, L_z is the distance between the heat source and heat sink centers, which is half of the total simulation domain length ($L_{\rm tot}$; see Fig. 2). The inset summarizes the calculated thermal conductivities of c-Si based on SW(GGA), with the available experimental values (Refs. 24 and 36) for comparison.

chosen conditions have been proven to be sufficient to provide reasonable results for all cases considered.[13]

We calculated thermal conductivities at 500 K for three different sets of SW parameters. Here, the relatively high temperature (=500 K) was intentionally chosen to check the reliability of the modified parameter sets while minimizing (or avoiding) the possible errors associated with quantum corrections;[35] the corrections are only on the order of ≈7% at 500 K for the experimental value (=645 K) of the Debye temperature. After quantum corrections, the calculated κ values of $82.88 \pm 5.36\ \mathrm{Wm^{-1}K^{-1}}$ and $83.84 \pm 7.71\ \mathrm{Wm^{-1}K^{-1}}$ based on SW(GGA) and SW(LDA), respectively, are in good agreement with the experimental value of 76.2 $\mathrm{Wm^{-1}K^{-1}}$,[24] while SW(ORI) leads to a considerable overestimation ($124.97 \pm 14.02\ \mathrm{Wm^{-1}K^{-1}}$). This result clearly demonstrates that the modified parameter sets derived from both GGA and LDA forces can describe reasonably well the thermal conductivity of Si; we expect that the force-matching approach can also be applicable to other materials. The calculated κ values (after quantum corrections) based on SW(GGA) at 300 and 400 K are also listed in the inset of Fig. 3. The overall good agreement with experiment suggests that the force-matched SW potentials would be a reliable choice for describing Si thermal transport properties in the temperature regime.

Figure 4 shows calculated phonon density of states (DOS) based on the modified and original parameters sets, together with relevant experimental data for comparison. For each case, the vibrational modes were determined by diagonalizing a Hessian matrix obtained from numerical differentiation of analytical forces that were calculated by displacing all constituent atoms (in a 512-atom cubic supercell) in the x, y, and z directions by 0.02 Å. The phonon spectrum is composed of four branches, such as longitudinal acoustic (LA), transverse acoustic (TA), longitudinal optical (LO), and transverse optical (TO). The force-matched potentials [SW(GGA) and SW(LDA)] reproduce the relative positions of the four peaks reasonably well, as observed in earlier experiments;[37,38] on the other hand, the original parameter

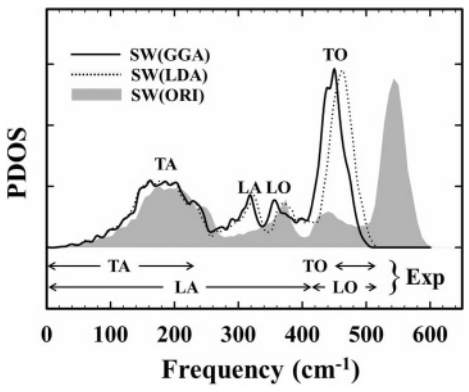

FIG. 4. Phonon density of states (PDOS) calculated based on different sets of SW parameters, as indicated; each of which consists of four longitudinal acoustic (LA), transverse acoustic (TA), longitudinal optical (LO), and transverse optical (TO) branches. For comparison, the relative positions of the four phonon branches extracted from experimental phonon-dispersion relations (Refs. 37 and 38) are also presented, as indicated.

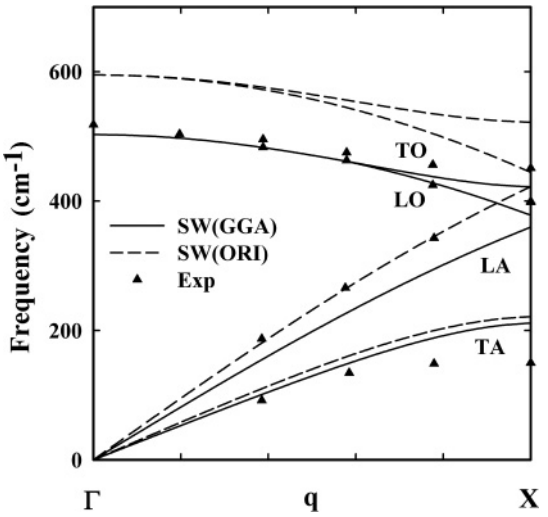

FIG. 5. Phonon dispersion for c-Si along high-symmetry directions. The SW(GGA) and SW(ORI)-based calculations were performed using the GULP (General Utility Lattice Program) computer program (Ref. 39). The solid and dashed lines correspond to the modified [SW(GGA)] and original [SW(ORI)] parameter sets, respectively. Triangles indicate experimental data from Ref. 38.

set [SW(ORI)] yields the upshifted frequencies (blue shift). The blue shift of the phonon branches is directly related to the increase of phonon group velocity; hence, SW(ORI) is expected to cause overestimation of thermal conductivity, according to the kinetic theory, $\kappa \propto \nu C_v l$, where υ is the group velocity of acoustic branches, C_v is the specific heat of phonons per unit volume, and l is the mean free path of phonons.[24]

Finally, we compared the phonon dispersion relations of c-Si from SW(GGA)/SW(ORI)-based calculations using the GULP computer program.[39] As shown in Fig. 5, the most noticeable difference between the SW(GGA)- and SW(ORI)-based dispersion curves occurs in the description of optical branches. The SW(ORI) significantly overestimates the optical frequencies while the SW(GGA) and experimental values are in good agreement; the highest optical frequency of 502.57/514.48 $\mathrm{cm^{-1}}$ (at Γ), as estimated from the SW(GGA)/SW(LDA) calculations, is much closer to the experimental measure[38] of 518.0284 $\mathrm{cm^{-1}}$, compared to the SW(ORI) value of 594.76 $\mathrm{cm^{-1}}$. The optical frequency overestimation may lead to the reduced phase space for phonon-phonon scattering, as the three-phonon phase space tends to be inversely related to the characteristic phonon frequency scale determined by the highest optical frequency.[40,41] As a result of the reduction of three-phonon umklapp scattering processes, the SW(ORI) likely causes a significant overestimation of the thermal conductivity at room temperature and above where phonon scattering dominates.[42] The results unambiguously suggest that the improved prediction of thermal conductivity by the modified SW(GGA)/SW(LDA) parameter sets is largely due to their tendency to yield a better fit to the phonon frequencies, as compared to the original SW(ORI) parameter set.

IV. SUMMARY

We present optimized parameter sets for the SW interatomic potential that provide significant improvements in estimation

of the lattice thermal conductivity of Si, over the original SW parameter set. Among seven SW parameters, the three most relevant ones (σ, ε, and λ) were adjusted to obtain a better fit of DFT (within the GGA and LDA) calculations of the lattice spacing as well as the restoring forces for displacements of a lattice atom in c-Si. With the modified parameter sets based on the GGA (LDA) calculations, NEMD simulations yield 82.88 ± 5.36 (83.84 ± 7.71), 109.24 ± 6.88, and 136.65 ± 9.15 $\mathrm{Wm^{-1}K^{-1}}$ after quantum corrections for bulk c-Si thermal conductivities at 500, 400, and 300 K, respectively, which are in good agreement with the respective experimental values of 76.2, 98.9, and 148 $\mathrm{Wm^{-1}K^{-1}}$, while the original SW parameter set results in significantly overestimated values (124.97 ± 14.02, 189.36 ± 15.28, and 243.99 ± 19.75 $\mathrm{Wm^{-1}K^{-1}}$). While lattice dynamics directly depend on the interatomic forces, we looked at the relative contributions of the two- and three-body forces to the difference between the modified [SW(GGA) and SW(LDA)] and original [SW(ORI)] potentials. For SW(GGA) and SW(LDA) with respect to SW(ORI), there is a significant reduction in the two-body forces ($\gamma_F = 0.65/0.70$ for GGA/LDA), while the three-body force reduction is relatively smaller ($\gamma_G = 0.91/0.88$ for GGA/LDA). The decrease of forces clearly indicates that SW(GGA) and SW(LDA) describe the Si lattice as softer than SW(ORI), thereby yielding lower thermal conductivities. In addition, our analysis of phonon density of states shows that the modified parameter sets reproduce the relative positions of the experimental peaks reasonably well, whereas the original parameter set gives the overall upshift in the phonon frequencies (blue shift). Our calculation results for phonon dispersion relations unambiguously suggest that the improved prediction of thermal conductivity by the modified SW(GGA)/SW(LDA) parameter sets is largely related to their tendency to provide a better fit to the phonon frequencies, as compared to the original SW(ORI) parameter set. Our study demonstrates that the force-matching-based parameterization can be a reliable choice for description of the lattice thermal conductivity of Si-based nanostructures; we also expect that the force-matching approach could be broadly applicable to other materials system.

ACKNOWLEDGMENTS

We acknowledge the Robert A. Welch Foundation (F-1535) for their financial support. We would also like to thank the Texas Advanced Computing Center for use of their computing resources.

*Corresponding author: gshwang@che.utexas.edu

[1] A. I. Hochbaum, R. Chen, R. D. Delgado, W. Liang, E. C. Garnett, M. Najarian, A. Majumdar, and P. Yang, Nature **451**, 163 (2008).
[2] A. I. Boukai, Y. Bunimovich, J. Tahir-Kehli, and J. R. Heath, Nature **451**, 168 (2008).
[3] G. F. Snyder and E. S. Toberer, Nat. Mater. **7**, 105 (2008).
[4] Z. Shao, S. M. Haile, J. Ahn, P. D. Ronney, Z. Zhan, and S. A. Barnett, Nature **435**, 795 (2005).
[5] A. Majumdar, Science **303**, 707 (2004).
[6] J. R. Lukes and H. Zhong, Trans. ASME: J. Heat Transfer **129**, 705 (2007).
[7] J. Che, T. Cagin, W. Deng, and W. A. Goddard III, J. Chem. Phys. **113**, 6888 (2000).
[8] P. K. Schelling, S. R. Phillpot, and P. Keblinski, Phys. Rev. B **65**, 144306 (2002).
[9] Y. H. Lee, R. Biswas, C. M. Soukoulis, C. Z. Wang, C. T. Chan, and K. M. Ho, Phys. Rev. B **43**, 6573 (1991).
[10] S. S. Mahajan, G. Subbarayan, and B. G. Sammakia, Phys. Rev. E **76**, 056701 (2007).
[11] J. Che, T. Cagin, and W. A. Goddard III, Nanotechnology **11**, 65 (2000).
[12] J. P. Crocombette and L. Proville, Appl. Phys. Lett. **98**, 191905 (2011).
[13] Y. Lee, S. Lee, and G. S. Hwang, Phys. Rev. B **83**, 125202 (2011).
[14] N. Yang, G. Zhang, and B. Li, Nano Lett. **8**, 276 (2008).
[15] I. Ponomareva, D. Srivastava, and M. Menon, Nano Lett. **7**, 1155 (2007).
[16] D. Donadio and G. Galli, Phys. Rev. Lett. **102**, 195901 (2009).
[17] Y. He, D. Donadio, J. H. Lee, J. C. Grossman, and G. Galli, ACS Nano **5**, 1839 (2011).
[18] A. Skye and P. K. Schelling, J. Appl. Phys. **103**, 113524 (2008).
[19] F. H. Stillinger and T. A. Weber, Phys. Rev. B **31**, 5262 (1985).
[20] J. Tersoff, Phys. Rev. B **37**, 6991 (1988).
[21] X. P. Li, G. Chen, P. B. Allen, and J. Q. Broughton, Phys. Rev. B **38**, 3331 (1988).
[22] M. Karimi, H. Yates, J. R. Ray, T. Kaplan, and M. Mostoller, Phys. Rev. B **58**, 6019 (1998).
[23] E. R. Cowley, Phys. Rev. Lett. **60**, 2379 (1988).
[24] C. Kittel, *Introduction to Solid State Physics*, 7th ed. (Wiley, New York, 2006).
[25] M. T. Dove, *Introduction to Lattice Dynamics* (Cambridge University Press, New York, 1993).
[26] Z. Jian, Z. Kaiming, and X. Xide, Phys. Rev. B **41**, 12915 (1990).
[27] L. Lindsay and D. A. Broido, Phys. Rev. B **81**, 205441 (2010).
[28] C. Flensburg and R. F. Stewart, Phys. Rev. B **60**, 284 (1999).
[29] F. Ercolessi and J. B. Adams, Europhys. Lett. **26**, 583 (1994).
[30] J. P. Perdew and Y. Wang, Phys. Rev. B **45**, 13244 (1992).
[31] G. Kresse and J. Furthmuller, *VASP The Guide* (Vienna University of Technology, Vienna, 2001).
[32] D. Vanderbilt, Phys. Rev. B **41**, 7892 (1990).
[33] S. Plimpton, J. Comput. Phys. **177**, 1 (1995).
[34] S. G. Volz and G. Chen, Phys. Rev. B **61**, 2651 (2000).
[35] J. E. Turney, A. J. H. McGaughey, and C. H. Amon, Phys. Rev. B **79**, 224305 (2009).
[36] R. K. Kremer, K. Graf, M. Cardona, G. G. Devyatykh, A. V. Gusev, A. M. Gibin, A. V. Inyushkin, A. N. Taldenkov, and H. J. Pohl, Solid State Commun. **131**, 499 (2004).
[37] G. Nilsson and G. Nelin, Phys. Rev. B **3**, 364 (1971).
[38] G. Nilsson and G. Nelin, Phys. Rev. B **6**, 3777 (1972).
[39] J. D. Gale and A. L. Rohl, Mol. Simul. **29**, 291 (2003).
[40] A. Ward, D. A. Broido, D. A. Stewart, and G. Deinzer, Phys. Rev. B **80**, 125203 (2009).
[41] L. Lindsay and D. A. Broido, J. Phys. Condens. Matter **20**, 165209 (2008).
[42] D. A. Broido, A. Ward, and N. Mingo, Phys. Rev. B **72**, 014308 (2005).